Sparse Step-Frequency MIMO Radar Design for Autonomous Driving

Shunqiao Sun, Lifan Xu and Nathan Jeong
Department of Electrical and Computer Engineering
The University of Alabama, Tuscaloosa, AL, USA

2021 IEEE Radar Conference (RadarConf21) | 978-1-7281-7609-3/20/$31.00 ©2021 IEEE | DOI: 10.1109/RadarConf2147009.2021.9455274

***Abstract*—To accommodate a high number of automotive radars operating at the same frequency band while avoiding mutual interference, we propose a sparse step-frequency waveform (SSFW) radar to synthesize a large effective bandwidth to achieve high range resolution profiles (HRRP). To mitigate high range sidelobes in the SSFW radars, we propose a joint sparse carriers selection and weighting approach, where the sparse carriers are first optimally selected via the particle swarm optimization (PSO) techniques, and then a weighting vector is optimized and applied such that the peak sidelobe level of range spectrum is minimized. As a result, targets with relatively small radar cross section are detectable without introducing high probability of false alarm. We extend the SSFW concept to multi-input multi-output (MIMO) radar by applying phase codes along slow-time to synthesize a large virtual array aperture. Numerical simulations are conducted to demonstrate the performance of the proposed SSFW MIMO radar.**

***Index Terms*—Automotive radar, multi-input multi-output (MIMO) radar, sparse step-frequency waveform, autonomous driving, interference mitigation**

I. Introduction

Radar sensors have found widespread applications in advanced driver assistance systems (ADAS), such as adaptive cruise control (ACC) and automatic emergency braking (AEB). According to National Highway Traffic Safety Administration (NHTSA) study, $37,461$ Americans died on the U.S. highways in 2016 as a result of automobile accidents [1], of which 94% were due to human error [2]. Recently, radar has emerged as one of the key technologies in autonomous driving systems. Automotive radar must provide high resolution in four dimensions, i.e., range, Doppler, and azimuth and elevation angles, yet remain a low cost for feasible mass production. High-resolution imaging radar is being developed to provide point clouds of the surrounding environment [3]–[6]. The target range resolution is determined by the signal bandwidth, whereas the Doppler resolution depends on the coherent processing interval (CPI). The angular resolution depends on the aperture of an antenna array, and the number of antennas is one of the most significant factors that determines the cost of the automotive radar. On the other hand, automotive radars need to be deployed on a massive number of vehicles, competing for the same frequency spectrum assigned for automotive radar applications. As the number of vehicles equipped with automotive radar increases, so does the probability of encountering mutual interference between these radar units. Without radio frequency interference (RFI) mitigation, therefore, automotive radars will suffer from performance degradation and eventually fail to function [6], [7].

By exploiting waveform orthogonality, multiple-input multi-output (MIMO) radar [8] is an attractive technique to enable automotive radar to achieve a large virtual array aperture at a low cost, and its advantage has been exploited by almost all major automotive suppliers, in their different types of radar products, including short-range radar, medium range radar, and long range radar [3], [9]–[11].

State-of-the-art automotive radar systems exploit frequency-modulated continuous-waveform (FMCW) signals at millimeter-wave frequencies [6], [12], [13] to enable high-resolution target range and velocity estimation, and can be implemented at a much lower cost than light detection and ranging (LiDAR). To achieve a high range resolution for autonomous driving, the transmit signals are designed to occupy a large bandwidth. For automotive FMCW radars, the frequency linearly sweeps over the entire large bandwidth, thereby making the signal susceptible to interference from other automotive radars. Another type of waveform that enhances waveform orthogonality is the recently developed pulse-modulated continuous-waveform (PMCW) [14]–[16]. PMCW radars take advantages of existing sequences with good auto-correlation and cross-correlation properties, previously developed for code-division multiple accessing (CDMA) communications, such as Gold, Kasami, and m-sequences [17], [18]. In PMCW radars, each automotive radar exploits a unique digital sequence to reduce mutual interference. However, PMCW radar has many implementation challenges. First, the sampling rate of the ADC should satisfy the Nyquist rule. As such, the high bandwidth required for high range resolution necessitates high-speed ADC and high-speed processing hardware.

Alternatively, step-frequency waveform (SFW) radar transmits a sequence of pulses with linearly increased carrier frequencies to synthesize a wide bandwidth while keeping a low instantaneous bandwidth of each pulse so low sampling rate analog-to-digital converters (ADCs) can be used [19]. However, there is range-Doppler coupling in the conventional SFW radars.

The sparse step-frequency waveform (SSFW) radar transmits a few pulses within a large bandwidth, where some frequencies are unused during a CPI [20], [21]. SSFW radar can avoid multiuser interference by skipping the spectrum bands that are occupied by other radars. However, use of SSFW

radars will increase range sidelobes and, as a result, targets with small radar cross section (RCS), such as pedestrian, may be obscured by high sidelobes of stronger targets.

In this paper, we propose a sparse step-frequency waveform MIMO radar system to synthesize high range resolution profiles (HRRP) for autonomous driving. The sampling rate of ADC is kept low, and the hardware cost is significantly reduced. To mitigate the high range sidelobe associated with random SSFW radar, we first optimally select the sparse carrier frequencies via particle swarm optimization technique and then applying an optimal weighting vector to the selected carriers to minimize the peak sidelobe level of the range spectrum so that targets with small RCS can be reliably detected without introducing high probability of false alarm. To synthesize a virtual array with large aperture, we extend the SSFW radar concept to MIMO radar by applying slow-time phase coding among each transmit antennas. Since only a small portion of the frequency spectrum is occupied, the proposed SSFW radar enables flexible coordination of spectrum utilization among multiple automotive radars with low mutual interference among automotive radars.

II. Sparse Step-Frequency-Based Automotive MIMO Radar

In this section, we address the problem of high-resolution target range estimation using SSFW signals with a small number of carrier frequencies. We start with a simple single-transmit single-receiver model, and then extend it to a MIMO setting in Section II-C where the waveform orthogonality is addressed with slow-time phase codes.

The transmit antenna transmits a sequence of N pulses whose carrier frequencies are sparsely distributed over the available bandwidth of B. The carrier frequencies $f_n \in [f_c, f_c + B]$, $n = 1, 2, \cdots, N$, are randomly chosen from the set $\mathcal{M} = \{f_n | f_c + h_n \Delta f, h_n \in \{1, 2, \cdots, P\}\}$ with $P = \lfloor B/\Delta f \rfloor$ equally spaced subcarriers, where Δf is the frequency step size and $\lfloor \cdot \rfloor$ denotes the floor function. The maximum unambiguous scope of HRRP and range resolution are respectively given by $R_u = c/(2\Delta f)$ and $\Delta R = c/(2P\Delta f) = R_u/P$. The duration of each pulse is T_p. After transmitted a burst of N pulses, the transmitters are turned off and the radar is switched to a receive mode. The total time duration of a burst cycle consisting of both transmit and receive modes is T, corresponding to the burst pulse cycle repetition frequency (CRF) of $f_{\text{CRF}} = 1/T$. One CPI consists of M burst cycles. Fig. 1 shows an example of one burst cycle with $N = 5$ pulses transmitted sequentially with carrier frequencies that are chosen from subset $\mathcal{M}$ with $P = 7$ frequencies. The n-th transmit pulse during the m-th burst cycle is expressed as

$$s(m, n, t) = \frac{1}{\sqrt{T_p}} \text{rect}\left(\frac{t - nT_p - mT}{T_p}\right) e^{j2\pi(t - nT_p - mT)f_n}, \tag{1}$$

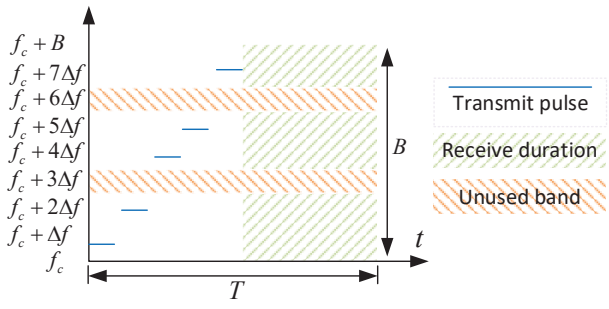

Fig. 1. Illustration of the sparse step-frequency radar with $N = 5$ sequentially transmitted pulses with carrier frequencies that are chosen as a subset of $\mathcal{M}$ with $P = 7$ frequencies.

where t is the fast time, and

$$\text{rect}\left(\frac{t - \tau}{T_p}\right) = \begin{cases} 1, & \tau - T_P \le t \le +\tau, \\ 0, & \text{otherwise.} \end{cases} \tag{2}$$

Each pulse has unit energy, i.e., $\int_0^{T_p} |s(n, m, t)|^2 \mathrm{d}t = 1$.

Consider K point targets in the far field, and the k-th target has range r_k, radial velocity v_k, and complex reflection coefficient β_k. The received signal of the n-th pulse at the m-th slow time corresponding to the k-th target is

$$\tilde{y}_k(m, n, t) = \beta_k s(m, n, t - 2r_k(t)/c), \tag{3}$$

where $r_k(t) = r_k(0) + v_k t$ and c is the speed of light. After demodulation, the n-th echo is sampled at the rate of $1/T_p$ in fast time $t_s(m, n) = mT + nT_p$ with $n = 1, 2, \cdots, N$, giving one sample per frequency step, expressed as

$$y_k(m, n) = \beta_k e^{-j\frac{4\pi}{c} f_n [r_k(0) + (mT + nT_p)v_k]}. \tag{4}$$

The sampled received signal for the n-th pulse is the superposition of the echoes from all K targets, i.e.,

$$\begin{aligned} y(m, n) &= \sum_{k=1}^{K} y_k(m, n) \\ &= \sum_{k=1}^{K} \beta_k e^{-j\frac{4\pi}{c} f_n [r_k(0) + (mT + nT_p)v_k]} \\ &= \sum_{k=1}^{K} \gamma_k e^{-j\frac{4\pi}{c}(f_c m T v_k + h_n \Delta f r_k(0))} \\ &\quad \times e^{-j\frac{4\pi}{c}(h_n \Delta f n T_p v_k + h_n \Delta f m T v_k + f_c n T_p v_k)}, \end{aligned} \tag{5}$$

where $\gamma_k = \beta_k e^{-j\frac{4\pi}{c} f_c r_k(0)}$.

We make the following assumptions:

A1) The unambiguous scope of HRRP defined as $c/(2\Delta f)$ should be larger than the scope of a range bin $cT_p/2$. This yields that $\Delta f < 1/T_p$.

A2) The range migration is negligible during one CPI, i.e., $v_k MT < cT_p/2$.

A3) Define $\xi_{m,n} = 2(2n\Delta f T_p + m\Delta f T + 2f_c T_p) v_k/c$. Considering the vehicle speeds in a typical autonomous

driving scenario, it is reasonable to assume $\xi_{m,n} \ll 1/P$ for $m = 0, \cdots, M-1$ and $n = 0, \cdots, P-1$.

A4) The Doppler shift is considered constant in one burst cycle T because of the short duration of the burst pulses.

A. Range and Doppler Estimation in SSFW Radar

Range estimation can be achieved by applying inverse discrete Fourier transform (IDFT) to the fast-time samples. The range resolution is determined by the frequency bandwidth. Traditional step-frequency radar systems require $N = P$ pulses to achieve a range resolution of R_u/P. For the proposed sparse step-frequency approach, we use $N < P$ pulses and still achieve the same range resolution of R_u/P.

Stack the samples of one CPI with M burst cycles as matrix $\mathbf{Y} = [\mathbf{y}_1, \cdots, \mathbf{y}_M] \in \mathbb{C}^{P \times M}$. Each column contains fast-time samples $\mathbf{y}_m = [y(m,1), \cdots, y(m,P)]^T$ for $m = 1, \cdots, M$, where $(\cdot)^T$ stands for transpose. For the unused frequency carrier subset $\bar{\mathcal{M}}$ with $\left|\bar{\mathcal{M}}\right| = P - N$, the samples $y(m,i), i \in \bar{\mathcal{M}}$, are zero. The rows of $\mathbf{Y}$ indicate the slow-time. Applying IDFT to the m-th column, we obtain

$$\begin{aligned} F_m(l) =& \frac{1}{P}\sum_{n=0}^{P-1} y(m,n)\, e^{j2\pi \frac{l}{P} n} \\ =& \frac{1}{P}\sum_{k=1}^{K} \gamma_k e^{-j\frac{4\pi}{c} f_c m T v_k} \times \sum_{n=0}^{P-1} e^{j2\pi\left(\frac{l}{P} n - \frac{2r_k(0)}{c} h_n \Delta f\right)} \\ & \times e^{-j2\pi\left(\frac{2h_n \Delta f n T_p v_k + 2h_n \Delta f m T v_k + 2 f_c n T_p v_k}{c}\right)}. \end{aligned} \tag{6}$$

For the step-frequency radar, $f_n = f_c + h_n \Delta_f$ and $h_n = n$ with $n = 0, 1, \cdots, P-1$, so we have

$$\begin{aligned} F_m(l) =& \frac{1}{P}\sum_{k=1}^{K} \gamma_k e^{-j\frac{4\pi}{c} f_c m T v_k} \frac{1 - e^{j2\pi\left(\frac{l}{P} - \frac{2r_k(0)}{c}\Delta f - \xi_{m,n}\right)P}}{1 - e^{j2\pi\left(\frac{l}{P} - \frac{2r_k(0)}{c}\Delta f - \xi_{m,n}\right)}} \\ =& \frac{1}{P}\sum_{k=1}^{K} \gamma_k e^{-j\frac{4\pi}{c} f_c m T v_k} e^{j\pi(P-1)\left(\frac{l}{P} - \frac{2r_k(0)}{c}\Delta f - \xi_{m,n}\right)} \\ & \times \frac{\sin\left(\pi\left(\frac{l}{P} - \frac{2r_k(0)}{c}\Delta f - \xi_{m,n}\right)P\right)}{\sin\left(\pi\left(\frac{l}{P} - \frac{2r_k(0)}{c}\Delta f - \xi_{m,n}\right)\right)}. \end{aligned} \tag{7}$$

Under assumption (**A3**), i.e., $\xi_{m,n} \ll 1/P$, it can be verified that, when $l_k = 2r_k(0) P \Delta f / c$, the amplitude of $F_m(l)$ achieves its maximum values (assuming the reflection coefficients of all K targets have the same magnitude). The target range can be calculated as $r_k(0) = c l_k/(2P\Delta f) = \Delta R l_k$. Note that, in the proposed SSFW radar, sidelobe levels increase at certain locations in the range spectrum due to the sparse spectrum utilization.

For each range bin l, the velocity estimation is obtained by applying discrete Fourier transform (DFT) to the obtained range spectra $F_m(l)$ for $m = 0, 1, \cdots, M-1$, given as

$$D_l(k) = \sum_{m=0}^{M-1} F_m(l)\, e^{-j2\pi \frac{k}{M} m}. \tag{8}$$

P-point IDFT for range estimation and M-point DFT for Doppler estimation provide $10\log_{10}(PM)$ dB SNR enhancement [6]. This SNR enhancement is considered as a processing gain which significantly benefits the angle estimation.

It is noted that compressive sensing (CS) algorithms can be effectively applied to estimate the target range in the SSFW radar from sparse step-frequency signals. However, the CS approach has an off-grid issue [22].

B. Range Sidelobe Optimization via Joint Sparse Carrier Selection and Weighting

As we discussed earlier, since the carrier frequencies are uniformly divided and randomly chosen, the range spectrum would have high sidelobes. As a result, targets with a small RCS may be obscured by the range sidelobes of stronger targets.

We introduce a joint two-phase optimization technique to achieve desirable range sidelobe level. The sparse carrier frequencies among the set $f_n \in [f_c, f_c + B]$ are first optimally selected using the the particle swarm optimization (PSO) technique [23] such that the peak sidelobe level (PSL) of the range spectrum is minimized. In the following step, we introduce a complex weight vector to further minimize the range spectrum PSL.

To obtain the optimal subcarriers and weight vector, we discretize the entire unambiguous range R_u into a fine grid of Q points, r_q, $q = 1, \cdots, Q$, separated by ΔR, and set $r_f = R_u/2$ as the range corresponding to mainlobe. The sidelobe area is then described by set $\mathcal{Q} = \{r_1, \cdots, r_f - \Delta R, r_f + \Delta R, \cdots, R_u\}$. Define a range steering vector with respect to range r_q as $\mathbf{b}(r_q) = [b_1(r_q), \cdots, b_P(r_q)]^T$, where

$$b_n(r_q) = \begin{cases} e^{-j2\pi \frac{2r_q}{c} f_n}, & \text{if } f_n \in \mathcal{M}, \\ 0, & \text{if } f_n \notin \mathcal{M}. \end{cases} \tag{9}$$

A fitness function F_n is used to evaluate PSL under a specific subcarrier selection. The subcarriers selection problem can be modeled as

$$\arg\max_{f_n} F_n(b_n(r_q)). \tag{10}$$

PSO provides a heuristic way to solve the optimization problem with integer variables [23]. Each subcarrier represents a particle and a population consists of N particles. The moderate populations are generated randomly from our solution space $\mathcal{M}$ to ensure a feasible solution. To select subcarriers to achieve desirable F_n, an update rule is defined as:

$$\begin{cases} V_i^{t+1} = \omega^t V_i^t + c_1 r_1 (lbest_i^t - S_i^t) + c_2 r_2 (lbest_i^t - S_i^t) \\ S_i^{t+1} = S_i^t + V_i^{t+1} \end{cases}$$

for $i = 1, 2, \cdots, I$ and $t = 1, 2, \cdots, G$, where I is the population number and G is the iteration upper bound. This rule updates the populations' velocity and decides which subcarriers are feasible for the next iteration. V_i^t is the i_{th} population's current velocity, and its next time velocity will be V_i^{t+1}. The time-varying weight factor is denoted by ω, which

TABLE I
THE PSO PSEUDO ALGORITHM

Input:N, I, G, c_1, c_2 and velocity boundary
Initial:
1) randomly generate populations S
2) call fitness function F_n to evaluate every particle's fitness
3) define lbest and gbest
For t=1,2...G, do
1) update particles' velocity and selected subcarriers
2) call fitness function to evaluate F_n
3) update $lbest$ and $gbest$
End
Output: selected subcarriers

is decreasing with iteration and assures global convergence. $Hooke's$ constants c_1 and c_2, take the response to local and global performance, respectively. The coefficients r_1 and r_2 are randomly chosen from 0 to 1. The i-th population's optimum is $lbest_i$, and the optimum of whole populations is denoted as $gbest_i$ in the iteration process. The S_i is the i-th population. The pseudo algorithm of PSO is summarized in Table I. It should be noted that the PSO algorithm provides sub-optimal solutions for sparse carrier frequencies selection to minimize the range spectrum sidelobe level.

In the second step, we introduce a complex weight vector $\mathbf{w} = [w_1, \cdots, w_P]^T$ for the optimally selected sparse carriers obtained by PSO to further optimize the PSL of range spectrum. The power spectrum of ranges corresponding to sidelobe in $\mathcal{Q}$ is constrained to be below a threshold η determined by peak sidelobe level (PSL), i.e., $\eta = 10^{V_{\max}/10}$, where $V_{\max}$ is the maximum allowed PSL in dB. The weight optimization can be viewed as a range sidelobe minimization problem and is formulated as

$$\begin{aligned} &\min_{\mathbf{w},\alpha} \ \alpha \\ &\text{s.t.} \quad \left|\mathbf{w}^H \mathbf{b}\left(r_q\right)\right| \le \eta + \alpha, \quad r_q \in \mathcal{Q}, \\ &\qquad \mathbf{w}^H \mathbf{b}\left(r_f\right) = 1, \end{aligned} \tag{11}$$

where $(\cdot)^H$ denotes conjugate transpose. The above optimization problem is convex and can be solved efficiently via CVX toolbox [24].

C. Waveform Orthogonality for SSFW MIMO Radar

In one CPI, a total number of M burst pulse cycles are transmitted. All transmit antennas simultaneously transmit the SSFW waveform at the same sparse carrier frequencies. We adopt phase coding in slow-time to achieve waveform orthogonality via Doppler division multiplexing (DDM) [6]. Each pulse has the same phase code in one burst cycle, and the phase code varies with different burst pulse cycles. The phase code for the m_1-th transmit antenna is given as $x_{m_1}(m) = e^{j2\pi\alpha_{m_1}(m)}$ for $m_1 = 1, \cdots, M_t$ and $m = 1, \cdots, M$ [25]. To separate the m_1-th transmit signal at a receiver, after range IDFT, a slow-time Doppler demodulation is applied to all range bins corresponding to the same pulse. The demodulated outputs of the M burst pulse cycles are assembled into a vector, and its DFT yields the Doppler outputs.

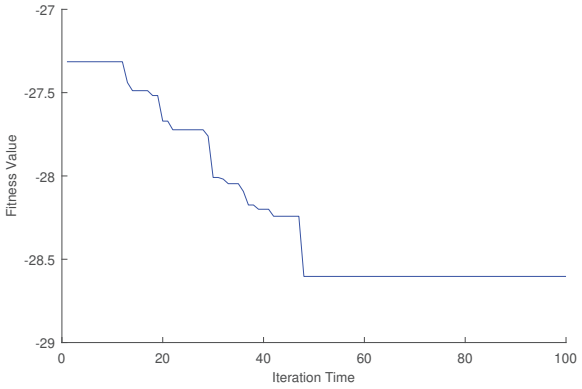

Fig. 2. PSL with iteration by PSO.

In this paper, we apply phase codes along the slow time so that the Doppler DFT of the interference can be distributed into the entire Doppler spectrum and treat it as pseudo noise with a low power spectrum. It is desired to minimize the peak interference residual (PIR) in the Doppler spectrum [26] computed using the discrete-time Fourier transform (DTFT) for $m_1 = 1, \cdots, M_t$, i.e.,

$$\text{PIR} = \max_{f, m_1 \neq h} \left| \sum_{m=1}^{M} e^{j2\pi\left(\alpha_{m_1}(m) - \alpha_h(m)\right)} e^{-j2\pi f m} \right|, \tag{12}$$

where $f \in \left[-\frac{1}{2} f_{\text{CRF}}, \frac{1}{2} f_{\text{CRF}}\right]$. Following Eq. (12), the cross-correlation of the spectra of two codes needs to be flat [26], since the Fourier transform of multiplication of the two codes in the time domain amounts to the convolution of their spectra.

Constant amplitude zero auto-correlation codes are good candidates for DDM. The DFT of a constant amplitude zero auto-correlation code has also a constant amplitude and zero auto correlation [27]. One of such examples is the Chu sequence [28], which is defined as $x_{m_1}(m) = e^{\frac{j\pi}{M} m_1 (m+1) m}$, $m_1 = 1, \ldots M_t$, $m = 1, \ldots, M$, where M is chosen as a prime number. In practice, the Chu sequence of prime length is first generated and then truncated into a length for efficient DFT computations.

The benefit of using slow-time phase coding is that the interference from other transmitters does not affect different range bins. The range resolution is determined only by the effective bandwidth of the synthesized SSFW waveform.

III. NUMERICAL RESULTS

In this section, we conduct numerical simulations to evaluate the performance of the proposed sparse spectrum approach for automotive applications.

A. Range Spectrum With Carriers Selection and Weighting

To demonstrate the performance of range and Doppler estimation using the proposed SSFW, for one burst cycle, $N = 300$ pulses are transmitted on carriers that are uniformly at carefully designed over $[f_c, f_c + B]$. The start carrier frequency is $f_c = 77$ GHz, and the effective bandwidth is set to $B = 200$ MHz, corresponding to range resolution of

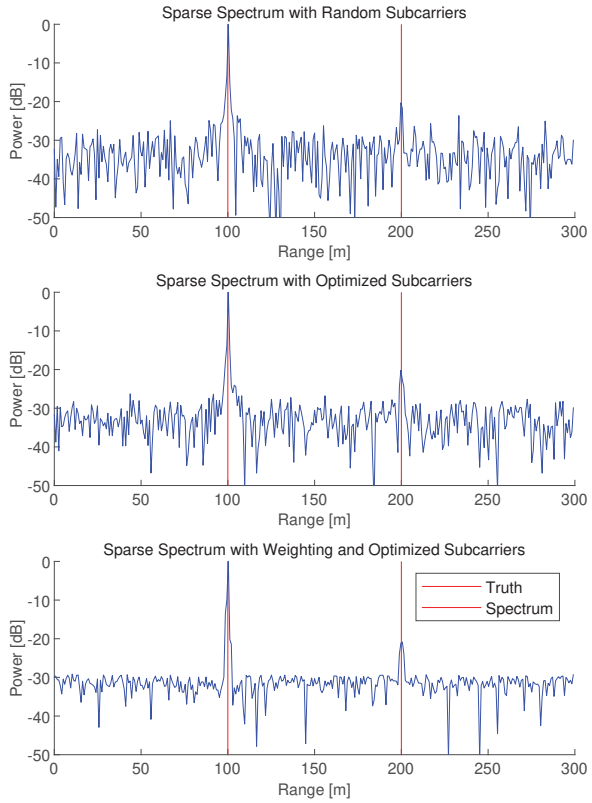

Fig. 3. Range spectrum comaprsion. Top: random sparse carriers. Middle: optimally selected carriers by PSO. Bottom: optimally selected carriers with weighting.

$\Delta R = 0.75$ m. The pulse duration is $T_p = 25$ ns and the step frequency is $\Delta f = 0.5$ MHz. The maximum unambiguous detectable range is $R_u = 300$ m. The burst cycle repetition interval is $T = 25$ μs. The maximum unambiguous detectable velocity is $v_{\max} = \lambda/(4T) = 38.96$ m/s. To measure the target velocity, $M = 300$ burst cycles are carried out with a dwell time of $MT = 7.5$ ms, rendering a velocity resolution of $\Delta v = \lambda/(2MT) = 0.26$ m/s. To achieve waveform orthogonality among transmit antennas, a Chu sequence of length $M = 307$ was generated and then truncated into length $M = 300$ for phase coding in slow-time. The SNR of the demodulated echo signals at receiver is set to 10 dB. Two targets are placed at 100 m and 200 m with normalized amplitude of 1 and 0.15, respectively. To suppress the high range sidelobes, subcarriers are optimally selected via the PSO algorithm. Figure 2 shows the convergence of PSO algorithm with parameters of N = 300, G = 100, c_1 = c_2 = 2, and 800 populations. After around 50 times iteration, an acceptable PSL, nearly -29 dB, has been achieved. In the following, the weights obtained by solving the optimization problem (11) are applied to the fast-time samples corresponding to sparse carrier frequencies obtained from PSO algorithm.

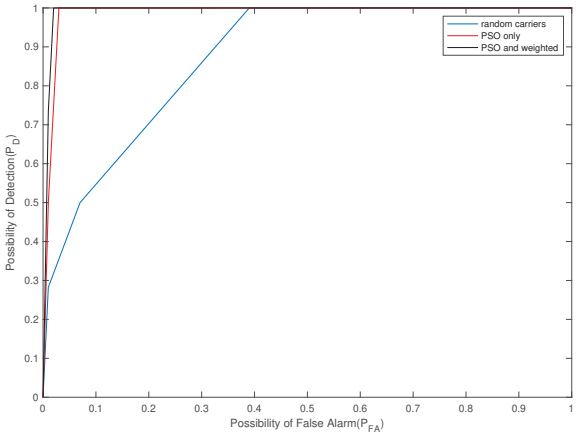

Fig. 4. Sparse step-frequency waveform radar detection performance comparison.

Figure 3 plots the comparison of range spectrum of the two targets under random sparse carrier frequencies allocation, optimal sparse carrier frequencies by PSO, as well as optimal carriers with weighting. It can be found that there are high range sidelobes under the random sparse carrier frequencies allocation, and as a result, the target with weak RCS might not be detected with introducing false alarm. On the contrary, the range sidelobes are significantly reduced under the sparse carriers optimally selected by PSO algorithm. The weighting vector helps further minimize the peak sidelobe level. As a result, the target of $R = 200$ m with low RCS can be reliably detected.

Figure 4 shows the receiver operating characteristic (ROC) curve to show the radar detection performance. Let $\hat{R}$ denote the estimated range of a target. If $\left|\hat{R} - R\right| \leq \varepsilon$ for a small value of ε, the target is detected. In the ROC curve of Fig. 4, we set $\varepsilon = 0.5$ m. It can be seen that under the optimally selected sparse carriers with weighting, the targets can be detected reliably with a high probability of detection (PD) of 100% at a very small probability of false alarm (PFA) of less than 4%, while under random sparse carrier allocation, the PD can be 100% only when PFA is larger than 38%.

B. Range-Doppler Spectrum Under Interference

In this section, we evaluate the range-Doppler spectrum of the proposed SSFW MIMO radar with slow-time phase coding via simulations. We assume there are $M_t = 2$ transmit antennas. A Chu sequence of length $M = 307$ is first generated and truncated into length of $M = 300$. We consider the scenario that the carrier frequencies are contaminated partially by interference. The interference is modeled as i.i.d. circular Gaussian random variable with zero mean and variance of $\sigma_{\mathbf{I}}^2$. The signal-to-interference ratio (SIR) in the m-th burst of pulses is defined as $\text{SIR} = 10\log 10\left(\frac{\|y(m,:)\|_2}{|\Lambda|\sigma_{\mathbf{I}}^2}\right)$, where Λ is an integer set consisting of sparse carriers that are contaminated by interference. In the simulation, we consider the case that frequencies in $[f_c + B - \Delta, f_c + B]$ are partially overlapped with other automotive radar, where $\Delta = 50$ MHz.

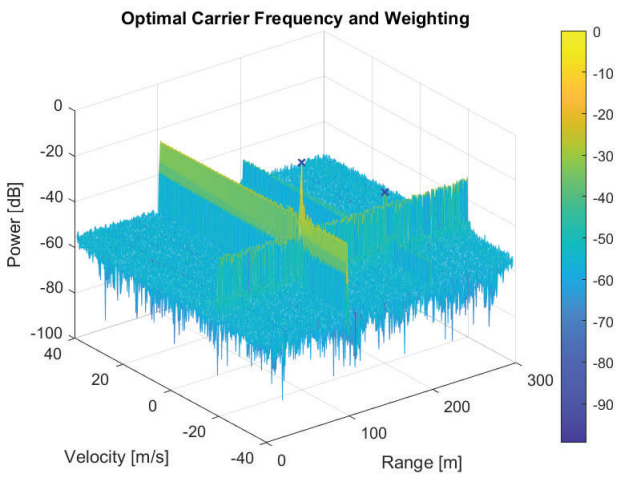

Fig. 5. Range Doppler spectrum of the SSFW MIMO radar for optimally selected carriers with weighting. Here, symbol $\times$ denotes the ground truth.

Figure 5 plots the range-Doppler spectrum of the two targets at ranges of $R_1 = 100$ m and $R_2 = 200$ m, with the same velocity of $v = -20$ m/s. The SIR is set to SIR $= 10$ dB. All the other radar parameters are the same as those listed in Section III-A. It can be found that the effect of interference is to increase the noise level of range-Doppler spectrum. Under the Chu sequence, the waveform residual from other transmit antenna is equally distributed over the whole Doppler spectrum corresponding to each target range bin. When partial carriers are contaminated by interference, the two targets can be detected reliably under the optimally selected carriers and weighting, i.e., the SSFW MIMO radar is robust to interference.

IV. Conclusions

In this paper, we developed a new automotive radar system utilizing a thinned frequency spectrum to synthesize a large effective bandwidth for high range resolution profiles. To avoid the situation that targets with small RCS may be masked by the high range sidlobes, we optimally selected the carriers and applied an optimal weighting vector such that the peak sideloble level was minimized. Numerical simulation verified that the proposed automotive radar yields high performance for range estimation with low-cost.

References

[1] U.S. Department of Transportation's National Highway Traffic Safety Administration (NHTSA), "2016 fatal motor vehicle crashes: Overview," [Available Online] https://www.nhtsa.gov/press-releases/usdot-releases-2016-fatal-traffic-crash-data, Oct. 6, 2017.

[2] L. Ecola, S. W. Popper, R. Silberglitt, and L. Fraade-Blanar, "The road to prepared for a vision for achieving zero roadway deaths by 2050," RAND Corporation Report, [Available Online] https://www.rand.org/pubs/research_reports/RR2333.html, April 18, 2018.

[3] I. Bilik and *et al.*, "Automotive MIMO radar for urban environments," in *Proc. IEEE Radar Conf.*, Philadelphia, PA, May 2016.

[4] F. Meinl, M. Stolz, M. Kunert, and H. Blume, "An experimental high performance radar system for highly automated driving," in *Proc. Intl. Conf. Microwaves for Intelligent Mobility (ICMIM)*, Nagoya, Japan, Mar. 2017.

[5] S. Alland and *et al.*, "Virtual radar configuration for 2D array," U.S. Patent 9 869 762, Jan. 16, 2018.

[6] S. Sun, A. P. Petropulu, and H. V. Poor, "MIMO radar for advanced driver-assistance systems and autonomous driving: Advantages and challenges," *IEEE Signal Process. Mag.*, vol. 37, no. 4, pp. 98–117, 2020.

[7] S. Alland, W. Stark, M. Ali, and A. Hedge, "Interference in automotive radar systems: Characteristics, mitigation techniques, and future research," *IEEE Signal Process. Mag.*, vol. 36, no. 5, pp. 45–59, 2019.

[8] J. Li and P. Stoica, "MIMO radar with colocated antennas," *IEEE Signal Process. Mag.*, vol. 24, no. 5, pp. 106–114, 2007.

[9] S. Alland and J. Searcy, "Radar system and method of digital beamforming," U.S. Patent 2009/0085800, April 2, 2009.

[10] M. Wintermantel, "Radar system with improved angle formation," U.S. Patent 2011/0074621, Mar. 31, 2011.

[11] M. Schoor and *et al.*, "Method for operating a MIMO radar," U.S. Patent 2014/0347211, Nov. 27, 2014.

[12] S. Patole, M. Torlak, D. Wang, and M. Ali, "Automotive radars: A review of signal processing techniques," *IEEE Signal Process. Mag.*, vol. 34, no. 2, pp. 22–35, 2017.

[13] F. Engels, P. Heidenreich, A. M. Zoubir, F. Jondral, and M. Wintermantel, "Advances in automotive radar: A framework on computationally efficient high-resolution frequency estimation," *IEEE Signal Process. Mag.*, vol. 34, no. 2, pp. 36–46, 2017.

[14] W. V. Thillo and *et al.*, "Almost perfect auto-correlation sequences for binary phase-modulated continuous wave radar," in *Proc. European Radar Conf. (EuRAD)*, Nuremberg, Germany, Oct. 2013.

[15] A. Bourdoux, U. Ahmad, D. Guermandi, S. Brebels, A. Dewilde, and W. V. Thillo, "PMCW waveform and MIMO technique for a 79 GHz CMOS automotive radar," in *Proc. IEEE Radar Conf.*, Philadelphia, PA, May 2016.

[16] D. Guermandi and *et al.*, "A 79-GHz 2x2 MIMO PMCW radar SoC in 28-nm CMOS," *IEEE J. Solid-State Circuits*, vol. 52, no. 10, pp. 2613–2626, 2017.

[17] R. Gold, "Optimal binary sequences for spread spectrum multiplexing (corresp.)," *IEEE Trans. Inf. Theory*, vol. 13, no. 4, pp. 619–621, 1967.

[18] T. Kasami, "Weight distribution formula for some class of cyclic codes," *Report*, pp. 1–32, 1966.

[19] M. A. Richards, *Fundamentals of Radar Signal Processing, 2nd Ed.* New York, NY: McGraw-Hill, 2014.

[20] L. Zheng, Q. Liu, X. Wang, and A. Maleki, "ℓ_p-based complex approximate message passing with application to sparse stepped frequency radar," *Signal Processing*, vol. 134, pp. 249–260, 2017.

[21] K. V. Mishra, S. Mulleti, and Y. C. Eldar, "RaSSteR: Random sparse step-frequency radar," [Available Online] https://arxiv.org/pdf/2004.05720.pdf, April, 2020.

[22] Y. Chi, L. L. Scharf, A. Pezeshki, and A. R. Calderbank, "Sensitivity to basis mismatch in compressed sensing," *IEEE Trans. Signal Process.*, vol. 59, no. 5, pp. 2182–2195, 2011.

[23] N. Jin and Y. Rahmat-Samii, "Advances in particle swarm optimization for antenna designs: real-number, binary, single-objective and multiobjective implementations," *IEEE Trans. Antennas Propag.*, vol. 55, no. 3, pp. 556–567, 2007.

[24] M. Grant and S. Boyd, "CVX: Matlab software for disciplined convex programming, version 2.1," http://cvxr.com/cvx, Mar. 2014.

[25] V. F. Mecca, D. Ramakrishnan, and J. L. Krolik, "MIMO radar space-time adaptive processing for multipath clutter mitigation," in *Proc. IEEE Workshop on Sensor Array and Multichannel Processing (SAM)*, Waltham, MA, July 2006.

[26] N. Madsen and S. Cao, "Slow-time waveform design for MIMO GMTI radar using CAZAC sequences," in *Proc. IEEE Radar Conf.*, Oklahoma City, OK, April 2018.

[27] J. Benedetto, I. Konstantinidis, and M. Rangaswamy, "Phase-coded waveforms and their design," *IEEE Signal Process. Mag.*, vol. 26, no. 1, pp. 22–31, 2009.

[28] D. Chu, "Polyphase codes with good periodic correlation properties," *IEEE Trans. Inf. Theory*, vol. 18, no. 4, pp. 531–532, 1972.